Report outline

Introduction

1. *Cell lines characterization*
2. *Cellular radioresponse*
   a. *X-ray irradiation*
   b. *Ion-irradiation at Naples Tandem*
      i. *Biological sample preparation*
      ii. *Beam diagnostics and dosimetry*
      iii. *Experimental set up*
      iv. *Irradiation runs*
      v. *Experimental procedure and post-irradiation sample processing*
      vi. *Results*
         1. *Cell survival*
         2. *Radiation-induced premature senescence*
         3. *Optimization of chromosome harvesting and mFISH protocol*
   c. *Irradiation with ^{16}O beam at INFN-LNS*
      i. *Preliminary results for chromosome aberrations*
3. *Preliminary conclusions and activities for 2013*
4. *Modellization work by Pavia Unit*

Introduction

The MIMO-Bragg experiment aims at studying the induction of sub-lethal cytogenetic damage along the Bragg curve for several accelerated ion beams in human normal cell lines and at modeling such effects based on the ion track structure rather than the radiation energy loss rate (LET). The radiobiological effectiveness of charged particles has been extensively studied thus far some endpoints (mainly cell killing and oncogenic transformation, but also chromosomal aberrations and other forms of DNA damage) and for a few positions along the Bragg curve, but there exists a substantial lack of experimental data for sub-lethal effects in normal cell lines, such as radiation induced premature senescence as well as for other cytogenetic effects, along the whole Bragg curve. This translates in a scant knowledge of how the radiobiological effectiveness of charged particles varies as a function of the ion penetration depth since the LET, and hence the amount of complex, irreparable damage is not constant as the ions traverses the biological matter. This is of relevance for both radioprotection and hadrontherapy purposes. It is in fact the surviving damaged cell which poses a health hazard: while chromosome aberrations are a well-recognized biomarker of cancer risk, a hitherto overlooked sub-lethal effect, the so called Stress-Induced Premature Senescence (SIPS), has been recently attracting growing interest since its occurrence in healthy tissues and/or organs, for instance in hadrontherapy patients, may lead to tissue degeneration and organ function impairment, hence it represents one of the most interesting radiation-induced late non-cancer effects. Since most of the current radiobiological models with which charged particle action is explained are based on the LET rather than the ion track structure, the final objective of this research program will be the

construction of experimental "biological" Bragg curves for such sub-lethal effects and their incorporation in Monte-Carlo based simulations.

In this report, preliminary data from experimental and theoretical work carried out within the planned activity for the first year of the MIMO-Bragg research program will be presented. Main objectives foreseen for 2012 were the validation of the experimental set-up for biological sample exposure to different Z ion beams and the collection of radiobiologically relevant data to investigate end-of-track effects for ions of similar LET values (Naples unit), and the implementation of home-made codes for modelization of chromosome aberration induction (Pavia unit). The experimental work was carried out irradiating three human normal cell lines at the 3-MV Van de Graaf TTT-3 Tandem accelerator at the Physics department, Federico II Naples University, with proton, ^{12}C and ^{16}O ion beams, for a total of eight runs. A first experimental run at INFN-LNS cyclotron with ^{16}O ion beam was also carried out in December 2012.

1. Cell line characterization

Growth curves were constructed for the three cell lines used in this project (endothelial HUVEC cells, foetal fibroblasts AG1522, and epithelial MCF-10 cells), as shown in figs. 1-3. Each of the three chosen cell lines was best suited to study a particular endpoint. HUVECs lend themselves to the study of the onset of premature senescence since they exhibit a highly reproducible pattern of physiological ageing *in vitro*; MCF-10A cells, on the other hand, posses a rather stable karyotype, which makes them suitable for investigation of radiation-induced chromosome aberrations. Finally, since clonogenic survival represents the gol standard against which any radiobiologically relevant effect must be compared, AGO1522 were used for deriving cell survival dose-response curves being this system widely used to study lethal effects on normal tissues. However, survival was assessed initially also for HUVECs and MCF-10 as to provide a conceptual link between the three used cell lines and the assays employed.
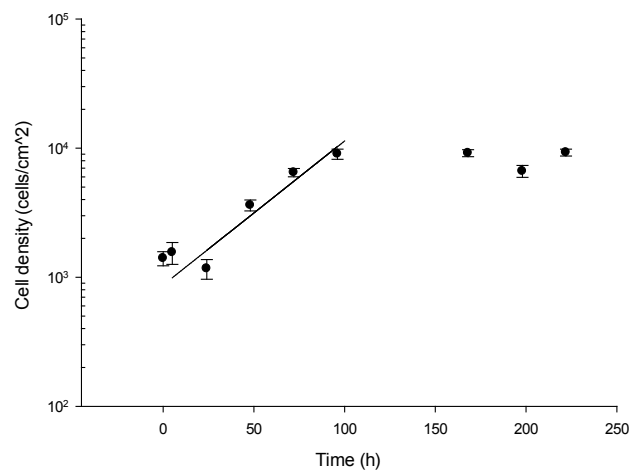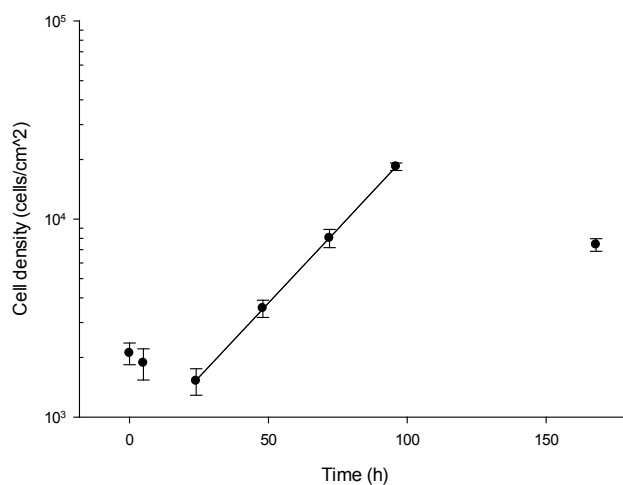

Fig.1: Growth curve for HUVEC cell line

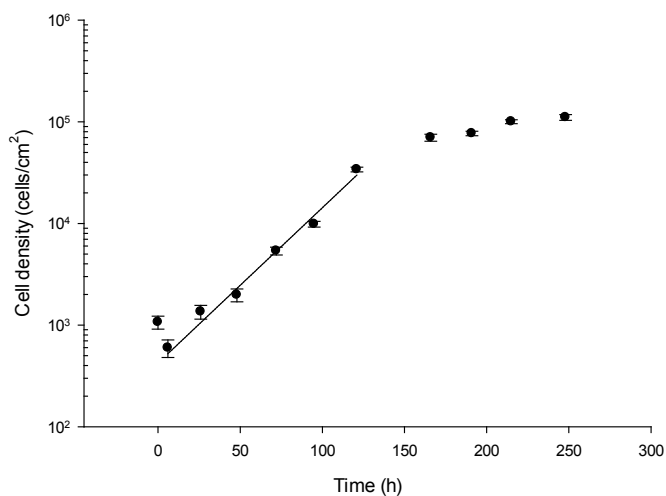Fig. 2: Growth curve for AGO1522 cells

Fig. 3: Growth curve for MCF10 cells

Fitting of experimental data from the exponential part of the curves allowed to estimate the mean doubling times for these cell lines under eh optimized growth conditions (table 1). Also reported are the typical plating efficiency (PE) values obtained for such cells, which reflect their proliferative potential to be used for control samples.

Cell line	T_d (h)	PE (%)
AGO1522	27 ± 7	10
HUVEC	20.1 ± 0.1	11
MCF-10	19.7 ± 1.1	60

Table1: Doubling time (T_d) e and plating efficiency (PE) for the cell lines used

2. Cellular radioresponse

a. X-ray irradiation

Cellular response to low-LET radiation (x-rays) was studied in terms of loss of cloning efficiency (clonogenic assay). This was necessary to define the relative biological effectiveness (RBE) of charged particles. Cells were exposed while in their exponential growth phase to a radiogen x-ray machine at the Physics department , University of Naples Federico II. Cell survival data (surviving fractions or SF) were fitted to linear-quadratic curves $SF = e^{-(\alpha D + \beta D^2)}$ where D represents radiation dose. The obtained curves are shown in figs. 4-6.
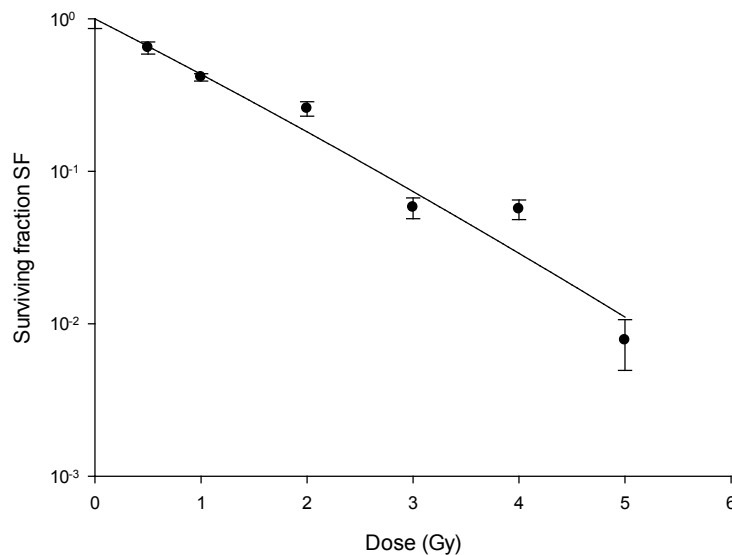

Fig. 4: Clonogenic dose-response for HUVEC following x-rays: experimental points are the mean of two irradiations, with relative standard error of the mean.
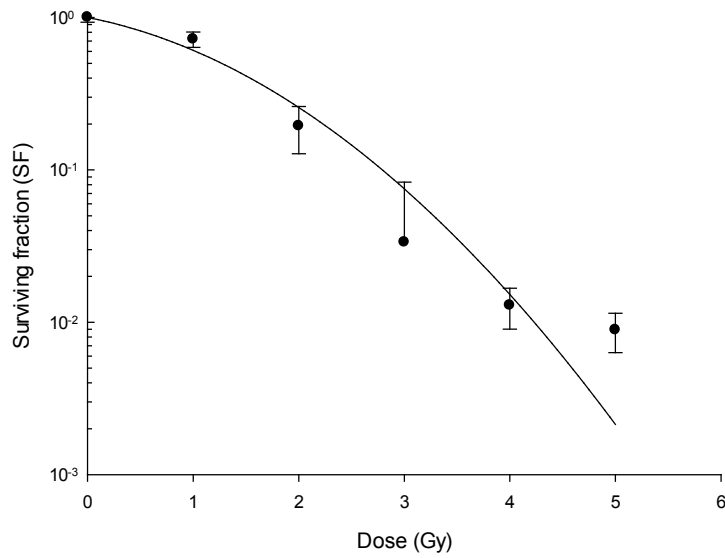
Fig. 5: Clonogenic survival of AGO1522 cells following x-rays (shown data are from two separate experiments)
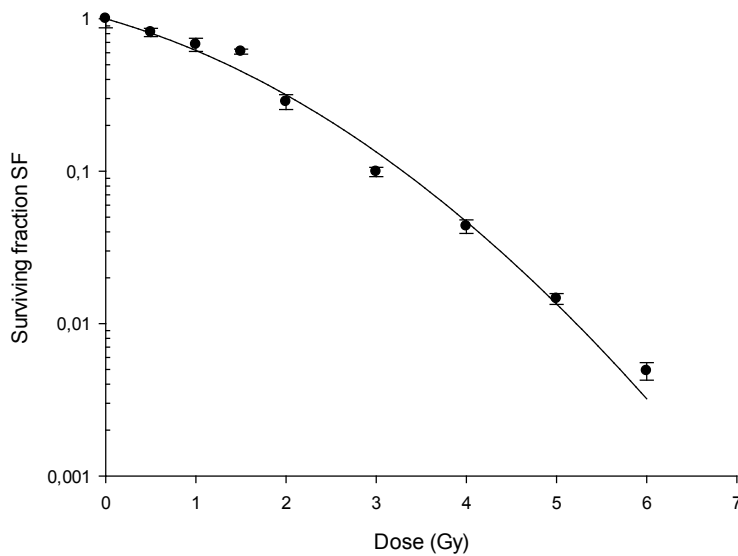

Fig. 6: Clonogenic cell survival for x ray-irradiated MCF-10 cells. Data refer to three separate irradiations.

Table 2 shows the fit parameters α and β. It has to be noted that HUVECs yielded the most radiosensitive response, basically lacking the typical "shoulder" at low doses, which indicates sub-lethal repairable damage; conversely, MCF-10 cells appear to be the most radioresistant ones.

Cell line	α (Gy^{-1})	β (Gy^{-2})
AGO1522	0.3 ± 0.2	0.18 ± 0.07
HUVEC	0.82 ±0.12	0.02 ± 0.04
MCF-10	0.38 ± 0.10	0.096 ± 0.02

Table 2: Linear-quadratic model parameters following exposure to reference radiation (x-rays)

b. *Ion-irradiation at Naples Tandem*

   i. *Biological sample preparation*

In order to be exposed at the Tandem, cells had to be plated onto purposely made pyrex cylinders (h=2.5 cm, d= 1.1 cm), whose base consisted of 1.5-μm thin mylar foil to which the cylinder had been glued by oven-cured araldite (fig. 7). The relatively low energies of the ion beams accelerated at Tandem allowed us to explore the radiobiological properties of end-of-range particles. Hence, it was critical to optimize and standardize the cells' growth conditions, such as the plating densities, as well as the time of seeding prior to exposure as to obtain a uniform cell monolayer. This was necessary as to minimize the uncertainty on the energy straggling of the ions close to the Bragg peak. Because of the different growth rates in vitro exhibited by the three cell lines as previously described (table 1), different cell seeding densities and time intervals before irradiation were determined for each cell line. Thus, for MCF-10 cells 5×10^4 cells/cylinder were seeded 72 h prior to exposure in the case of chromosome damage measurements; for HUVEC and AGO1522 cells, instead, 4×10^4 cells/cylinder had to be inoculated 24 h prior to exposure and determination of cellular senescence and clonogenic survival, respectively.
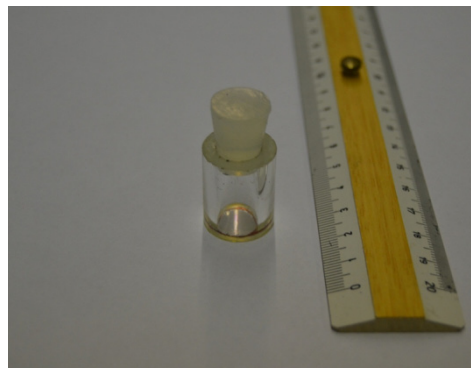

Fig. 7: In this picture a cylinder used as cell holder for exposure at Naples Tandem is shown. The cap guarantees sterility during as cells were taken from the biology lab to the accelerator room.

Measurement of thickness of the cell monolayer by means of a confocal microscope located at the Stazione Zoologica A. Dohrn, Naples, was unsuccessful because of technical reasons (sub-optimal intracellular fluorescent dye uptake, unsatisfactory z-stack focal planes acquisitions, etc.). At the

time this report was being written, we managed to optimize a staining protocol and are in the process of repeating such measurements. Based on literature data for similar cell lines grown on the same mylar substrate, we assumed an average cell thickness ranging between 10 to 12 μm for calculation of residual particle range. The energy values for the ion beams that were used (see below) were therefore chosen as to ensure that the cells were exposed at least at two different positions in the close proximity of the Bragg peak.

ii.   Beam diagnostics and dosimetry

For the ion beam irradiation a 3 MV TTT-3 Tandem was used at the Physics Department of the University of Naples Federico II (fig. 8). Beam intensity was monitored with the aid of several Faraday cups placed along the beamline. A fast, remotely controlled shutter is placed downstream after the last cup and just before the beam is collimated. To ensure uniform exposure of the cylinder base where cells were grown, the beam had to be diffused: a scattering gold foil was used (~450 μg/cm^2).
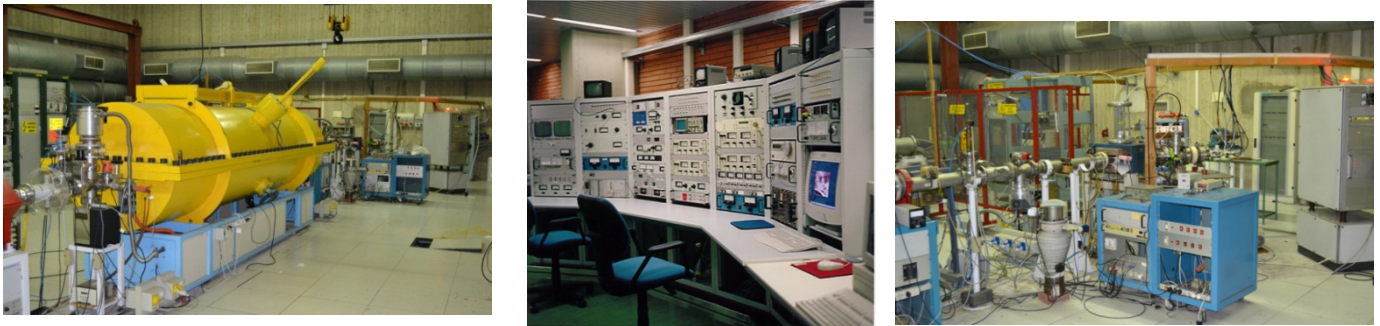

Fig. 8: On the left, the tank filled with the insulating SF$_6$ gas is shown; the main console (middle); on the right a view of the switching magnet

Energy spectra and dosimetry measurements were carried out by means of Si detectors and solid-state nuclear track polycarbonate CR-39. Particle fluence was determined by CR-39 etching and particle tracks were counted on 20 randomly chosen fields (fig. 9) under a 32X magnification objective (each scored field had an area of 1.25 10^{-4} cm^2): the mean particle count was used to correct retrospectively the nominal value of the administered dose.
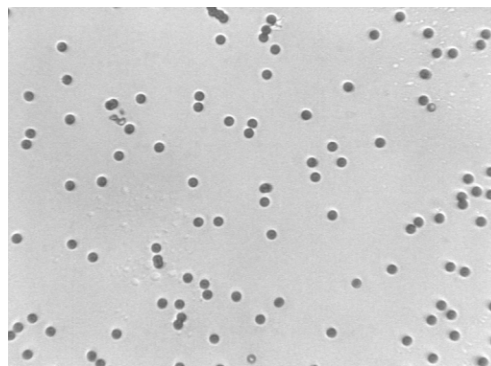

Fig. 9: A typical field as seen under light microscope for a CR-39 detector after chemical etching by KOH 10 N (80°C for 30 min). The tracks here shown are from a carbon ion beam

Energy spectra (fig. 10) were used to calculate by means of the SRIM2011 software (www.srim.org) the energy through the scattering foil and the particle incident energy and LET. The beams were substantially monoenergetic, as confirmed by the acquired spectra, whose resolution (FWHM) was in the order of a few tens of keV.

Beam uniformity was checked by three Si detectors (sensitive area of 25 mm^2 and 14 keV nominal resolution), 7-cm distant and symmetrical with respect to a central detector, in whose position after the cells' holder was placed during irradiations. The counts from the lateral detectors and those from the central one represented the calibration factor that was used to estimate the fluence and hence the dose to be administered during the cells exposure.
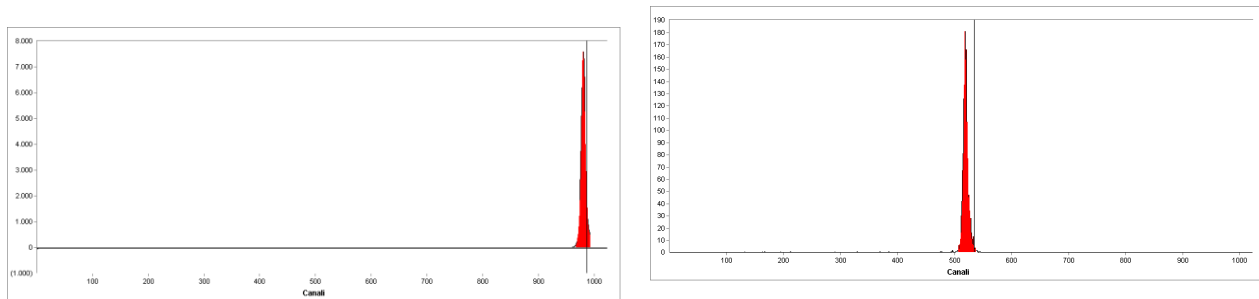

Fig. 10: Examples of spectra acquired by a dedicated multichannel analyzer during the experimental run of May 2012 with carbon ions. In red are shown the ROI delimiting the peak. On the left the spectrum, for carbon ions of nominal energy 15 MeV (terminal voltage V_T 2.5 MV, charge status q=+5); on the right it is shown the spectrum obtained for 8.4 MeV carbon ion beam (V_T = 1.7, q=+4); in both cases the spectra refer to the beam emerging past the scattering foil. By means of calibration with pulse generator and three peak radioactive emitter (^{239}Pu+2^{41}Am+^{244}Cm), the energy values were associated to the position of peaks in the multichannel.

iii.   Experimental set up

In previous years, radiobiological investigations performed at the dedicated beamline of the Naples Tandem had suffered from limitations, mainly imposed by the low energy with which ion beams could be accelerated, which resulted in the use of low-Z particles (protons, alphas and lithium). For the scientific scopes of this projects, it was therefore necessary to devise a new set-up which would significantly reduce the energy loss through the beam transport system. Part of such work was already been done in 2011 , thus making it possible to use ions up to fluorine. Such unprecedented Z values could be reached by changing the pre-existing set-up, where the beam was extracted in air at the window exit , passing through a 2.5-μm mylar foil and a few mm wide air chamber (which would add further uncertainty to the estimate of the actual energy loss before the ions reached the cell holder).

With the help of the Tandem laboratory personnel, the main technical novelty put in operation was the realization of a chamber where a pre-vacuum was achieved, which allowed the biological samples to be irradiated in rapid succession (without having to "break" the vacuum as previously necessary). Most importantly, the bean extraction in air was no longer necessary by creating a closing cap at the end of the beamline in which the cylinder holding the cells would serve itself as a vacuum tap. Such a solution allowed to "gain" several MeV since the beam energy was degraded

only by interaction with the gold scattering foil. This in turn allowed us to study the radiobiological properties of medium Z ions around their Bragg peak. Photos of the novel experimental set up are shown in fig.11.
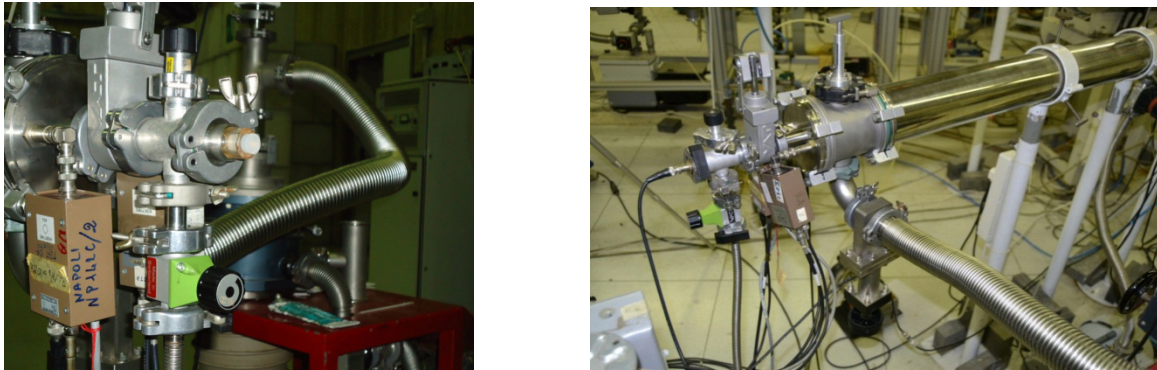

Fig.11: The exit beamline currently used at Naples accelerator for radiobiological studies. On the left it is shown the actual irradiation set up and the cell holding cylinder can be seen (the mylar on which cells are attached is facing the beam).Also visible is one of the lateral detector used to monitor on-line the particle counts on which the dose to be delivered is established. The picture on the right shows the beamline exit when the central detector replaces the cell holder during the dosimetry measurements, and the vacuum pumping system.

iv.   Irradiation runs

In 2012 eight irradiation runs have been performed at Naples Tandem. In some instances, only partial accomplishment of the planned experimental schedule could be achieved, for a number of reasons: in the January run, for example, a longer-than-expected maintenance schedule conflicted with the allocated beam time, forcing us to reduce the number of irradiated samples; in April, instability issues with the beam coupled with an accidents during the vacuum operations resulted in an abrupt end of the run. The June run was also prematurely ended because of a problem with the source due to inadequate cooling.

Overall, fully successful runs were conducted in March with protons, in May, July and November with ^{12}C beams and in December with ^{16}O. In tables 3-5 a synopsis of all ions, energies, LETs and residual range values are presented, divided per assay and per cell line. In each run, we planned to use two different energies for each ions in order to irradiate cells on two positions close to the end of the ion range. Each run lasted at least a week, with a preparatory phase dedicated to beam extraction, transport and dosimetry (paragraph ii), three days being necessary to irradiate all samples. Of course, time in advance was also necessary for cell seeding and cylinder preparations (paragraphs i and iii). On the same day of irradiation, biological samples were processed according to the protocols established for the assays used. Please note a caveat is represented by the fact that in some cases data were not available due to sub-optimal colony growth (clongenic assay) or chromosome harvesting (aberration assay).

Cell line	Beam	Energy (MeV)	LET (keV/μm)	Residual range (μm)
MCF-10	Protons*	0.8	27	20
	Protons*	0.7	30	15
	Protons*	0.6	34	11.5
	Carbon[1]	9.8	807	12.9
	Carbon[1]	12.2	741	15.9
	Carbon	12.8	726	16.7
	Carbon	5.9	934	8.3
	Carbon[2]	12.8	726	16.7
Huvec	Protons	0.8	27	20
	Protons	0.6	34	11.5
	Carbon	12.2	741	15.9
	Carbon	5.9	934	8.3
	Carbon	12.8	726	16.7
	Carbon	5.9	934	8.3
	Carbon[2]	12.8	726	16.7
AG1522	Protons*	0.8	27	20
	Proton*	0.6	34	11.5
	Carbon	12.2	741	15.9

Table 3: Runs for determination of cell survival. Energy is meant as incident on the cell monolayer and measured by detector prior to traversing the mylar sheet. LET and residual range values were obtained by calculations based on the incident energy. *Dosimetry affected by uncertainty due to malfunctioning of lateral detectors. [1] Run prematurely ended prior to irradiation at lower energy.[2] Run prematurely ended prior to irradiation with lower energy

Cell line	Beam	Energy (MeV)	LET (keV/μm)	Residual range (μm)
Huvec	Protons*	0.8	27	20
	Protons*	0.6	34	11.5
	Carbon[1]	12.2	741	15.9
	Carbon	12.8	726	16.7
	Carbon	5.9	934	8.3
	Carbon[2]	12.8	726	16.7
	Oxygen	6.2	1128	7.2

Table 4: Runs for determination of cellular premature senescence. Conventions for labels and superscripts are as for the table above.

Cell line	Beam	Energy (MeV)	LET (keV/μm)	Residual range (μm)
MCF10	Protoni*	0.6	34	11.5
	Carbon	12.8	726	16.7
	Carbon	5.9	934	8.3
	Oxygen	6.2	1128	7.2
	Oxygen	15.0	1370	14.4

Table 5: Runs for determination of chromosome aberrations. Conventions for labels and superscripts are as for the table above.

v.   Experimental procedure and post-irradiation sample processing

Following physical characterization of the beam (detector calibration, energy spectra acquisition, lateral detector count normalization), cylinders were emptied from cell growth medium (cylinder is placed horizontally at the beam exit window), sealed with a sterile rubber cap and taken to the Tandem room. The typical dose rate during irradiations was about 2 Gy min^{-1}, which given the relatively low doses used (the highest dose used being 6 Gy in the case of cell survival dose-response curves), which guaranteed that cells were not affected by lack of medium. Immediately after irradiations, cylinders were taken back to the biology laboratory and processed according to the different assays. To avoid errors due to cells attached at the edge of the cylinder basis, which could receive no dose because of glue residuals, a concentric cylinder had been realized which was inserted in the main cylinder as to collect by trypsinization only the cells attached in the central area, counted and plated at different concentrations for the construction of cell survival curves (fig.12) .

For senescence measurement, cells were processed the next day, and split in two amounts for each dose: one portion of irradiated cells were plated in 35-mm petri dishes and subjected to histochemical assay for detection of beta-galactosidase activity (an enzyme which is acknowledged to be expressed exclusively by senescing cells). The remaining aliquot was seeded in ordinary tissue culture flasks and propagated for weeks (up to 2 months from radiation exposure) and assayed at regular time intervals as to study the time-course of radiation-induced senescence. Finally, cells destined to the study of radiation-induced chromosome aberrations, i.e. residual damage potentially inheritable to the progeny of surviving cells, were processed 24 h post-irradiation as to allow completion of damage repair and hence harvested according to classical cytogenetic protocols. Structural chromosome aberrations were revealed by whole-chromosome and multicolour Fluorescence in Situ Hybridization (FISH) techniques.
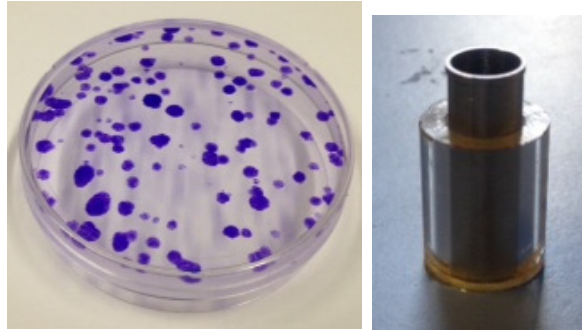
Fig.12: A typical petri dish with macroscopic colonies grown from single cell suspension for determination of clonogenic cell survival (left). Metallic cylinder used to select the cell population growing in the central area of the holding cylinder as to avoid spurious results due to unirradiated cells growing at the cell monolayer edge.

vi.   Results

1.Cell survival

Clonogenic survival data are shown following end-of-range proton irradiation at Naples tandem (figs. 13-14) . Table 6 recapitulates the beam incident energies and LET values, and the estimated residual ranges within exposed cells. For clarity sake, no data fitting curves are shown.

Energy (MeV)	LET (keV/μm)	Residual range (μm)
0.8	27	20
0.7	30	15
0.6	34	11.5

Tab. 6: Physical characteristics of the proton beams used. The energy is meant as the one incident on cells and measured as the beam emerged from the scattering foil, while LET and residual range values were calculated by SRIM2011.
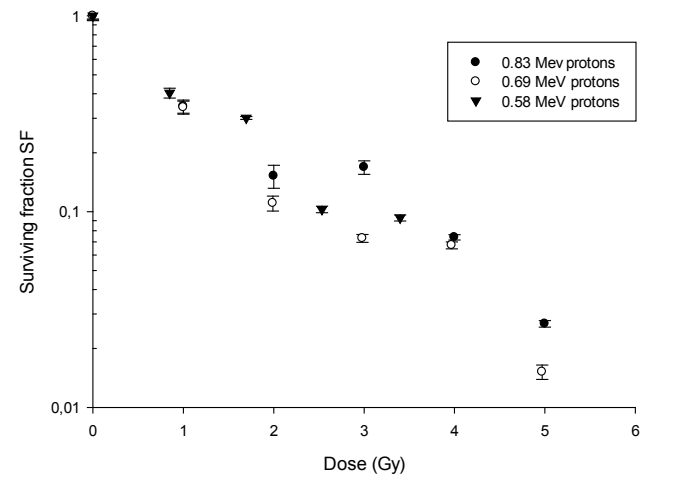
Fig.13: MCF-10A cell response to proton beams for different energies and residual ranges
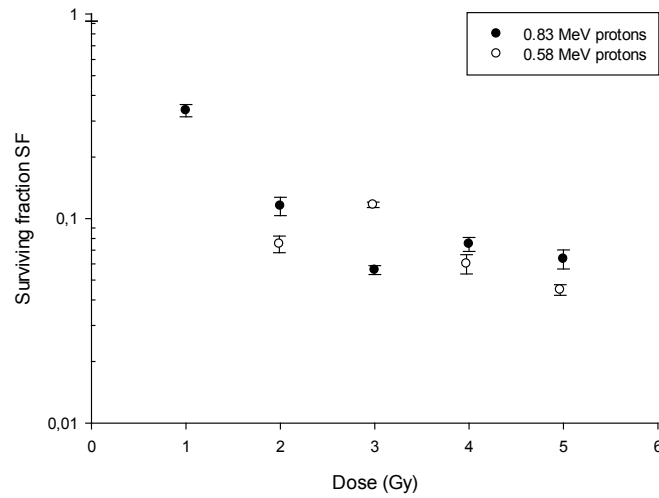
Fig.14: Clonogenic survival of HUVEC to protons closet o the Bragg peak

For comparison purposes with the reference low-LET radiation, the same data as shown above are plotted in fig. 15
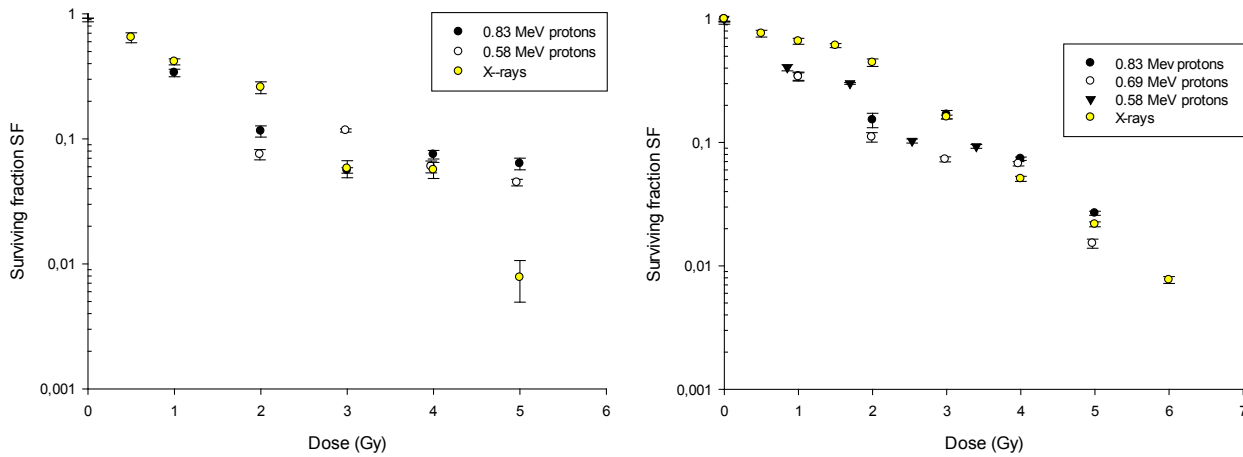

Fig. 15: The response of HUVEC (left graph) and MCF-10A cells (right graph) is shown together with the serviva measured after x-rays (yellow dots).

In figs. 16 and 17 clonogenic survival data obtained for the MCF-10A and HUVEC cell lines following ^{12}C ion beam irradiations are shown, with energy, LET and range values summarized in table 7.

Energy (MeV)	LET (keV/µm)	Range residuo (µm)
5.9	934	8.3
9.8	807	12.9
12.2	741	15.9
12.8	726	16.7

Tab. 7: Physical properties of the ^{12}C ion beams used
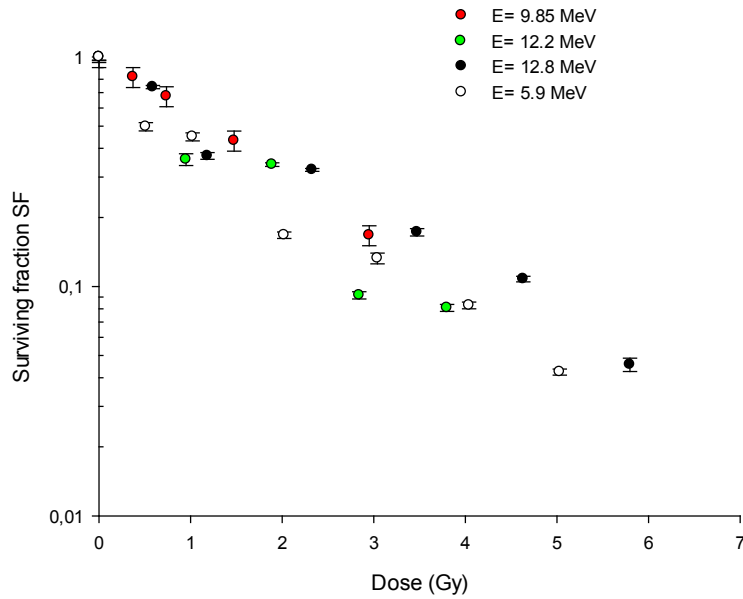
Fig. 16: Response of MCF10A cells to ^{12}C close to the Bragg peak.
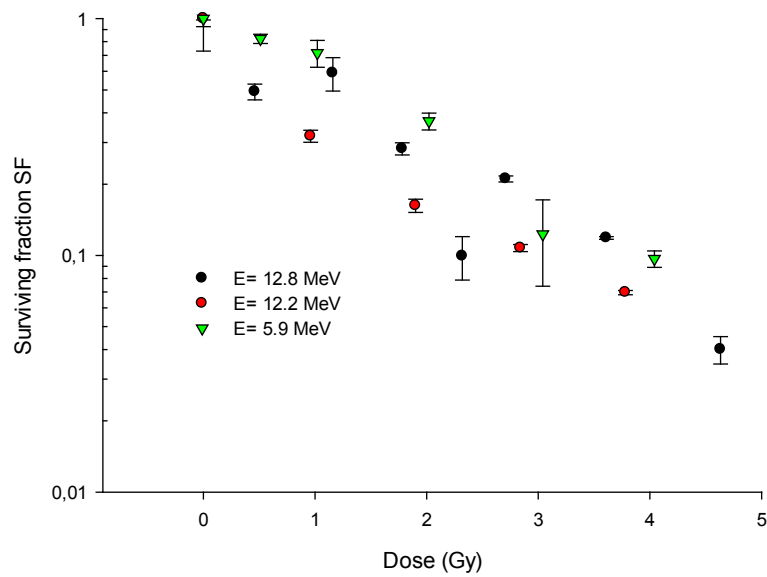
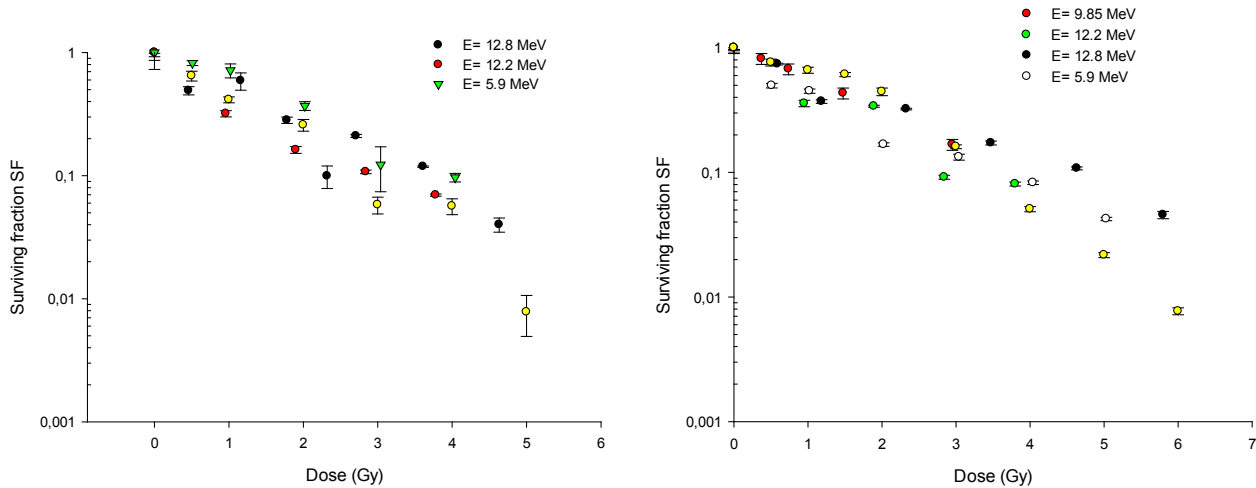Fig. 17: HUVEC survival data following exposure to ^{12}C ion beams

Fig. 18: As in the case of protons, cellular response for HUVEC (left) and MCF-10A (right) is plotted including data from x-ray irradiation to allow RBE estimate.

Cell survival data are also plotted for HUVEC and MCF-10A cells for carbon ions following irradiation with ^{12}C ion beams during July experimental run (fig.19): in this case, data were fitted to linear and linear-quadratic dose-responses to facilitate comparison of radiosensibility with x-rays.
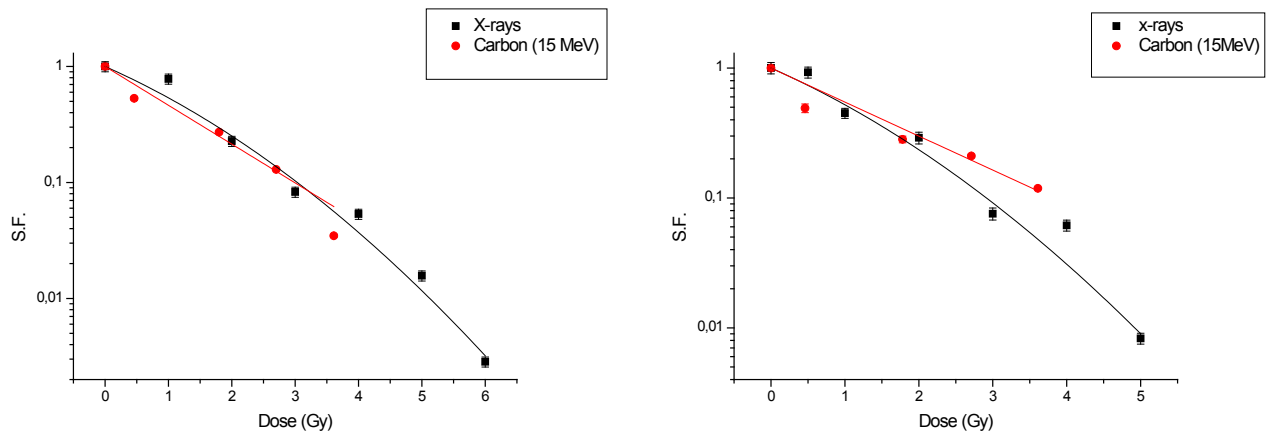

Fig.19: Clonogenc survival for MCF-10A (left) and HUVEC (right) following ^{12}C ion beam incident on cells with E=12.8 MeV. Black symbols and fit line refer to x-ray data for the same cell lines.

The radioresponse of HUVEC cell lines to a ^{12}C ion beam (incident energy 5.9 MeV) used during the run of November 2012 is shown in fig.20 together with data from x-ray irradiation.
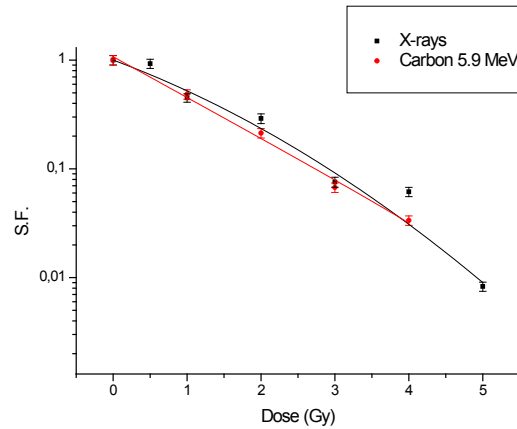
Fig.20: Clonogenic dose-responses following ^{12}C ion beam and x-rays for HUVEC (November 2012)

From the data above shown, it is possible a crude estimate of the RBE of protons and ^{12}C ions, whose values are shown in Table 8.

Particle (incident energy)	LET (keV/µm)	RBE$_{10\%}$
Protons (0.8 MeV)	27	1.04
Protons (0.6 MeV)	34	1.02
Carbon (12.8 MeV)	726	0.92
Carbon (5.9 MeV)	934	0.87

Table 8: Estimated RBE values for charged particles at various energies evaluated at 10% survival level

2.Radiation-induced premature senescence

Premature cellular senescence is a late-occurring effect following exposure to a variety of sub-lethal cytogenetic stressors, among which ionizing radiation has proven to be quite effective even at relatively low doses and particularly after charged particles. However, its onset in vitro has been poorly investigated for varying Z ion beams although its occurrence *in vivo*, of relevance in had therapy cancer patients, may compromise genome stability and physiological tissue homeostasis.
We have therefore studied this endpoint in HUVEC cells by means of the beta-galactosidase assay: senescing cells appear as green when looked at on light microscope (fig.21). Data were obtained following up irradiated cultures exposed to protons, ^{12}C and ^{16}O ion beam at the Naples Tandem accelerator and scoring between 500 and 1,000 cells per time and dose point on randomly chosen fields.
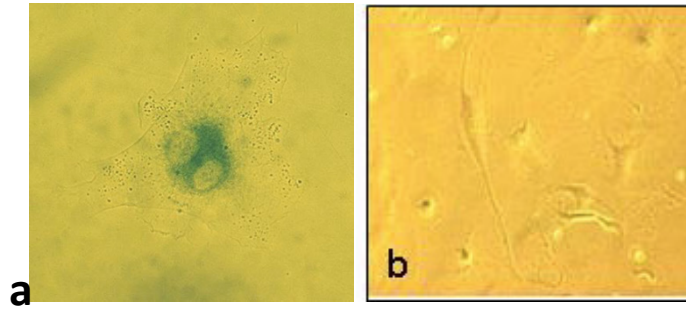
Fig. 21: Radiation-induced cellular senescence. Photo a) shows a binucleated cell expressing the typical coloration due to beta-galactosidase activity; b) characteristic morphology of senescing cells that look flattened and elongated
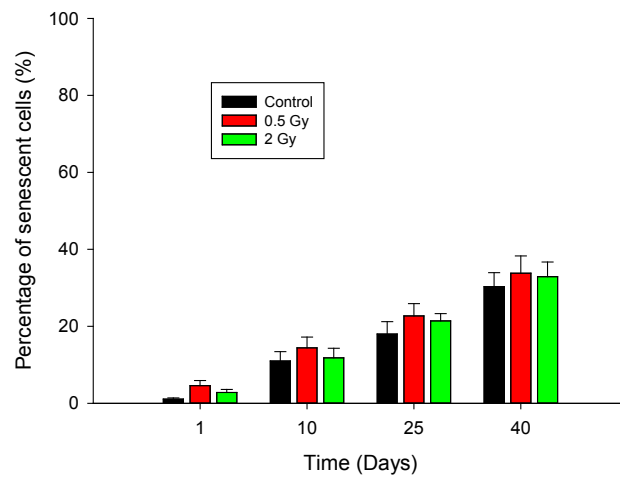

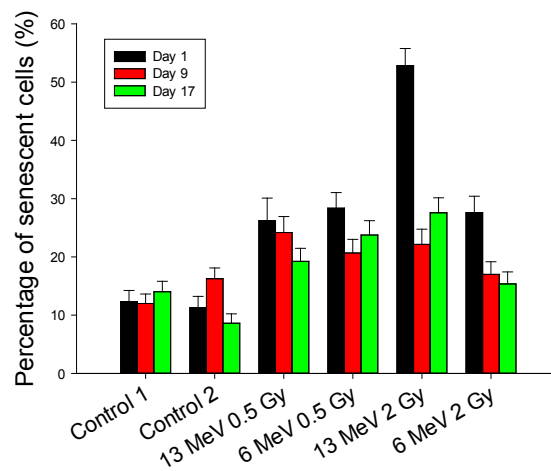Fig. 22: X ray-induced cellular premature senescence

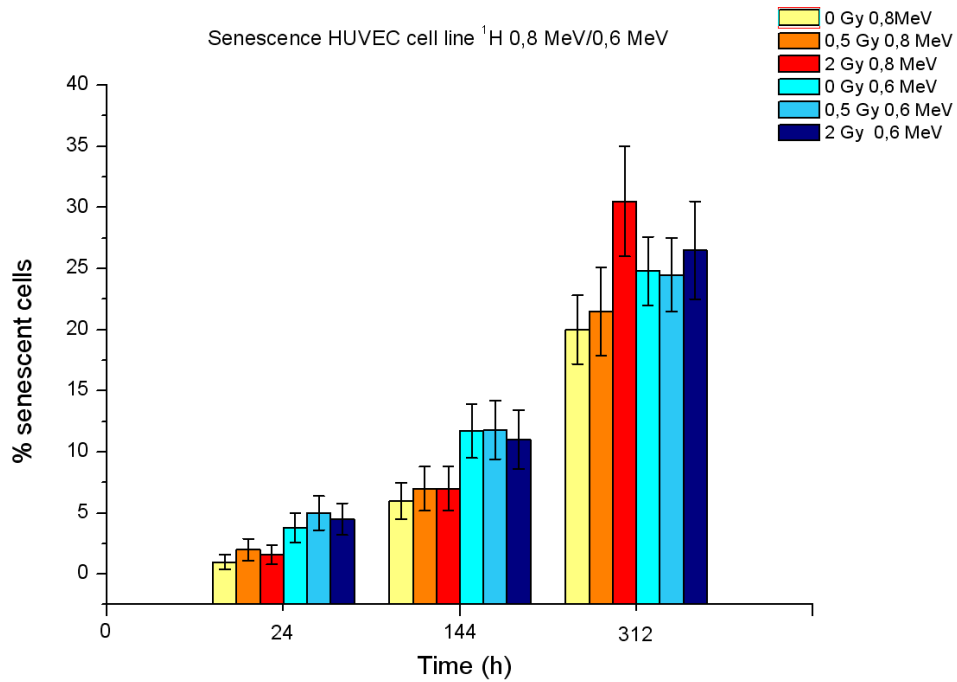Fig. 23: Induction of senescence by ^{12}C in beams of different energies.

Fig.24 Cellular senescence following proton irradiation (incident energies 0.8 and 0.6 MeV) for 0.5 and 2 Gy at 1, 6 and 13 days past exposure
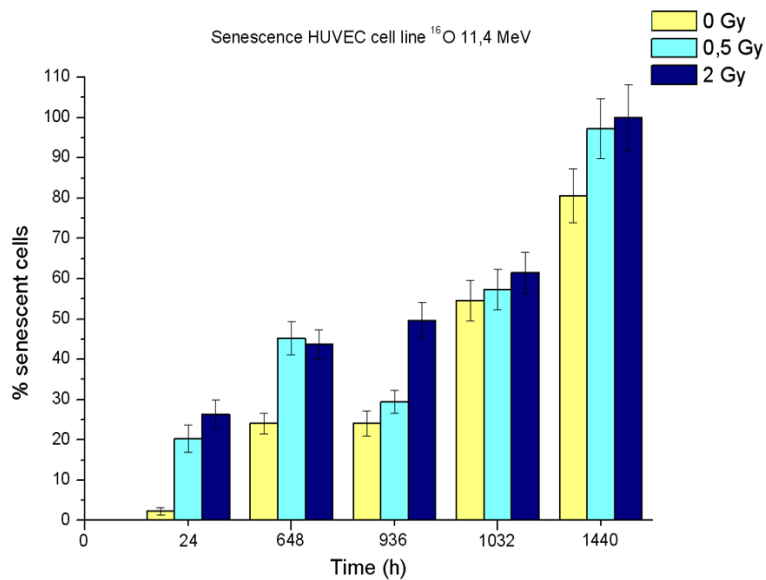

Fig. 25: Preliminary data from ^{16}O irradiation at Naples tandem (December 2012), with about 6.2 MeV incident energy (nominal accelerating energy from source 11.4 MeV). Cells were sampled at days 1, 27, 39, 43 and 60 past exposure

3.Optimization of chromosome harvesting and mFISH protocol

Calyculin A–based premature chromosome condensation (PCC) method was chosen to circumvent potential loss of information deriving from radiation-induced cell cycle delay had the conventional metaphase scoring been adopted. Since we had previously used this method on lymphocytes and not on adherent cell lines such as MCF-10A optimal concentrations and time of action for calyculin A had to be established. From the tests conducted, the best results in terms of condensation efficiency and quality of chromosome spreads were obtained with 50 nM of calyculin added 30 mins prior to harvesting. mFISH protocol was also optimized for our laboratory working conditions. Modification of the routine classifier necessary for karyotiping (Metasystem software, Germany) was necessary to adapt the pre-existing parameters (optimized for lymphocytes) to the cell line used. Satisfactory results were obtained for both hybridization and analysis (fig. 26).
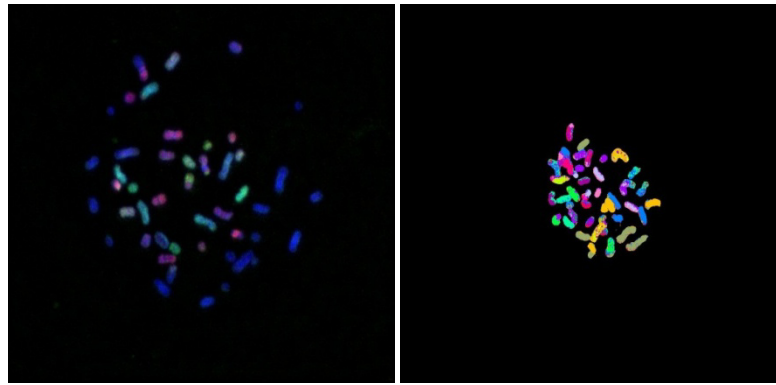

Fig. 26: mFISH performed on a PCC from MCF-10A cells (left) and image processing (false colour) for karyotype analysis (right)

Following the above described optimization for mFISH protocol, preliminary qualitative data were gathered for ^{16}O ion-irradiated MCF-10 cells.

c.   *Irradiation with ^{16}O beam at INFN-LNS*

i.*Preliminary results for chromosome aberrations*

Following the PAC meeting held at INFN-LNS, Catania, in June, a first experimental run was allocated in December 2012. A 60 MeV ^{16}O beam was used and premature cellular senescence and chromosome aberration inductions were studied at different positions along the Bragg curve (fig. 27). Cells were grown in standard tissue culture flasks and handled prior to and post irradiation at the LNS biology facility. Over 50 samples were irradiated. Sample positioning was achieved with resolution less than 50 microns, which greatly reduced the dose uncertainties. Positions (labeled as P1…P4) corresponded to estimated LET values of 68, 105, 409 and 769 keV/μm, respectively.
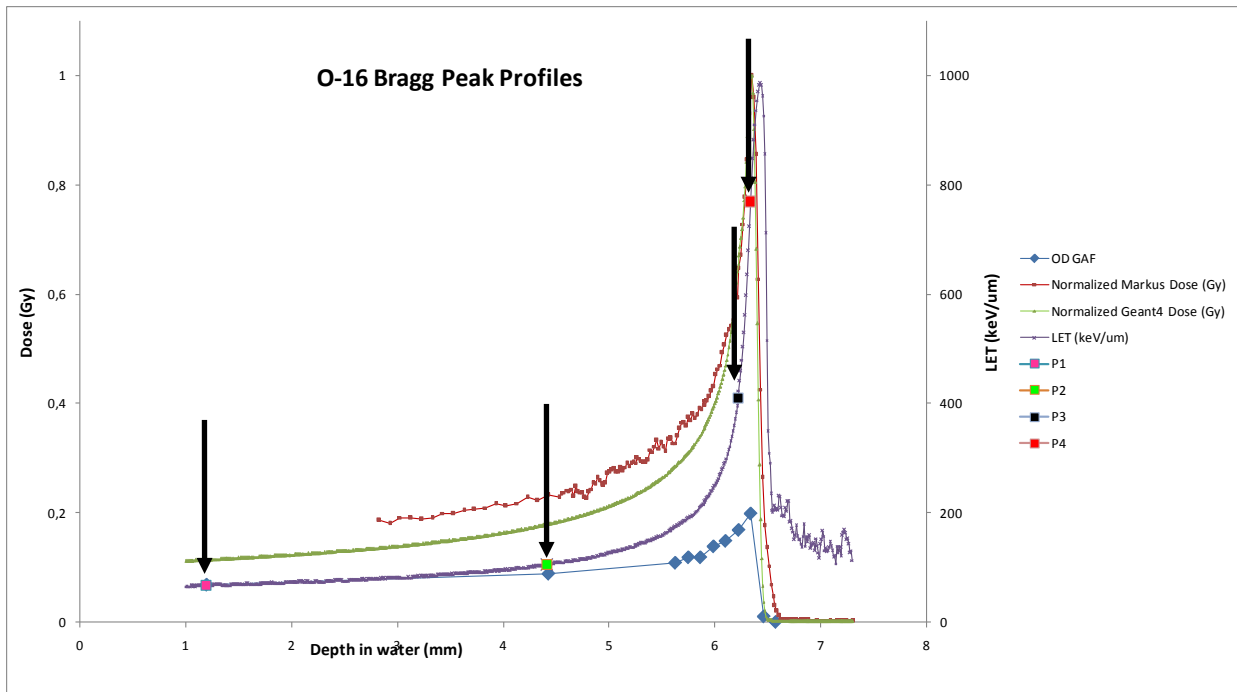
Fig. 27: Dose distributions (Markus chamber) and relative LET values (Geant4 simulations) for the ^{16}O ion beam. Sample positioning (arrows and squares) was verified by optically reading of Gafchromic films and comparing the qualitative dose profile with the quantitative measurements from the Markus chamber.

Here we report the results for conventional whole-chromosome FISH(fig. 28) and qualitative analysis by mFISH. For comparison, chromosome aberration data are also presented for x-ray irradiation.
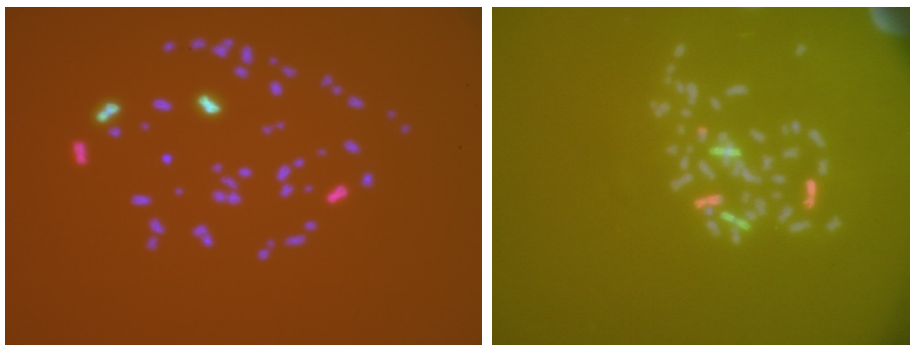

Fig. 28: Example of FISH: chromosomes 1 are painted with a green fluorescing fluorochrome (FITC) when UV illuminated, while the pair of homologue chromosomes 2 fluoresce in red/orange. A normal chromosome spread is shown on the left while an aberrant one exhibiting a translocation is pictured on the right.

Fig. 29 shows the data collected following exposure to x-rays: the fraction of aberrant cells provides an indication of the overall damage inflicted to DNA while the frequency of aberrations per cell reflects the burden of such damage on individual cells. Also the frequency of complex-type exchanges is plotted since such aberrations are recognized as a classical cytogenetic "signature" of exposure to high-LET radiations; finally, the pie charts represent how chromosomal damage is distributed at the used doses (0-4 Gy) for the main aberration categories scored (simple or complex exchanges, and fragments). In figs. 30-31 aberration data from FISH-painted whole chromosome analysis are shown for [16]O ion irradiation.
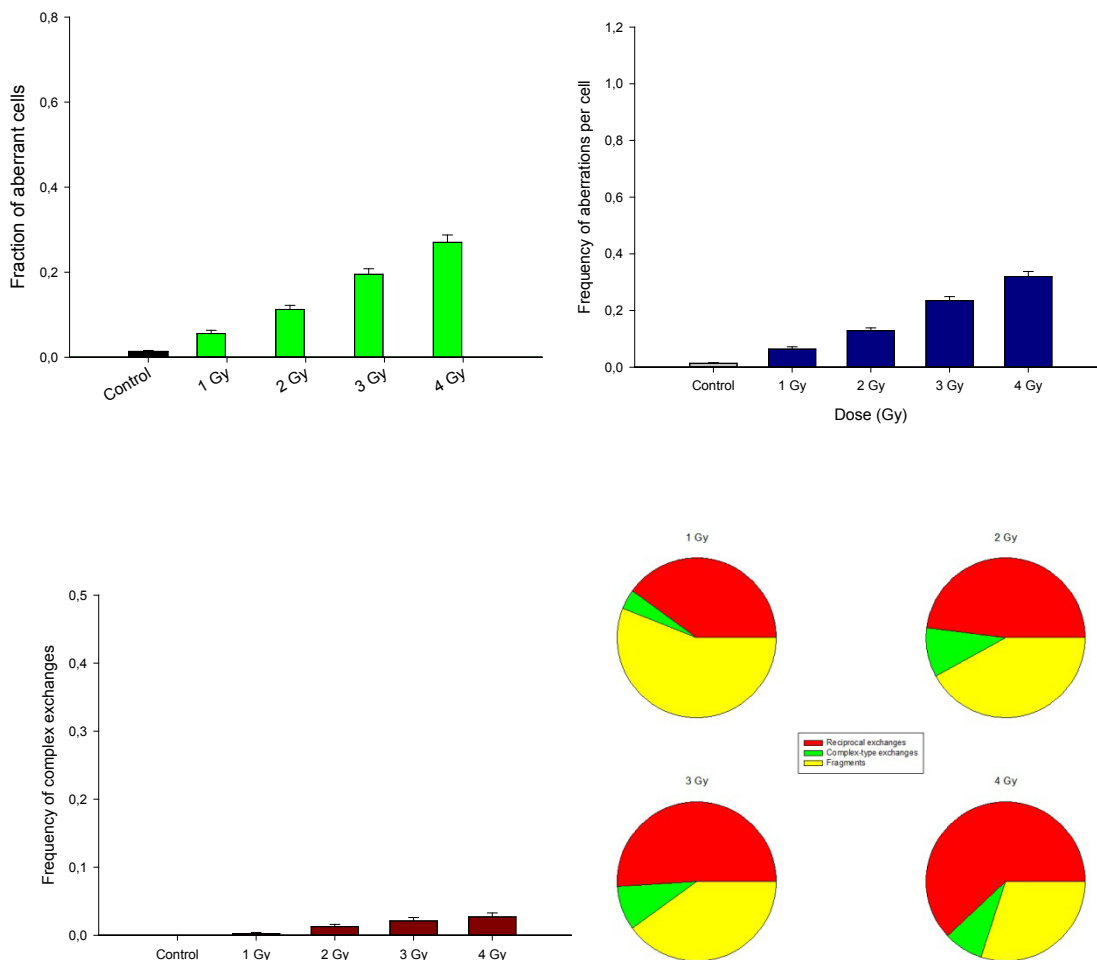

Fig. 29: Chromosomal damage induced by x-rays. The pie charts show the relative contributions to the overall pool of scored aberrations from three major categories of chromosomal rearrangements, i.e. reciprocal exchanges (red slices), complex-type exchanges (green) and fragments (yellow).

Fig. 30: Proportion of aberrant cells (left) and frequency of aberrations per cell (right) following [16]O ion-irradiation

Fig. 31: Frequency of complex-type aberrations after [16]O ion-irradiation of MCF-10A cells (above). The pie charts show the relative contributions to the overall pool of scored aberrations from three major categories of chromosomal rearrangements, i.e. reciprocal exchanges (red slices), complex-type exchanges (green) and fragments (yellow).
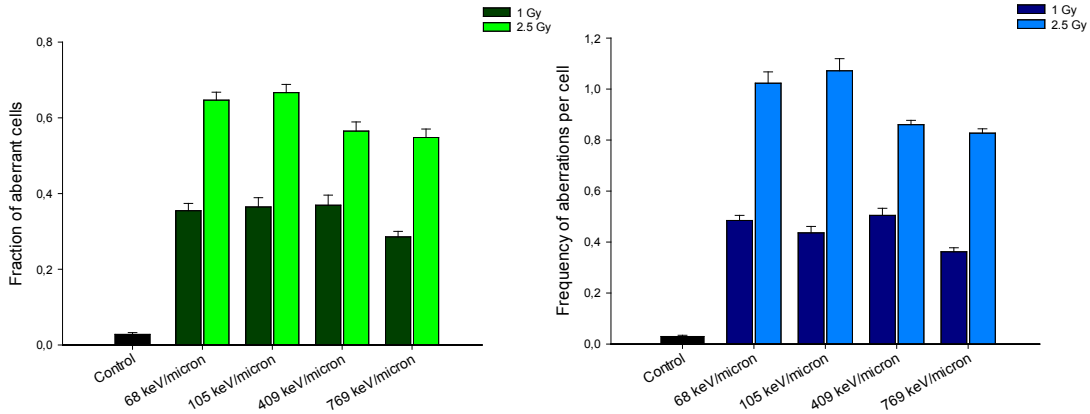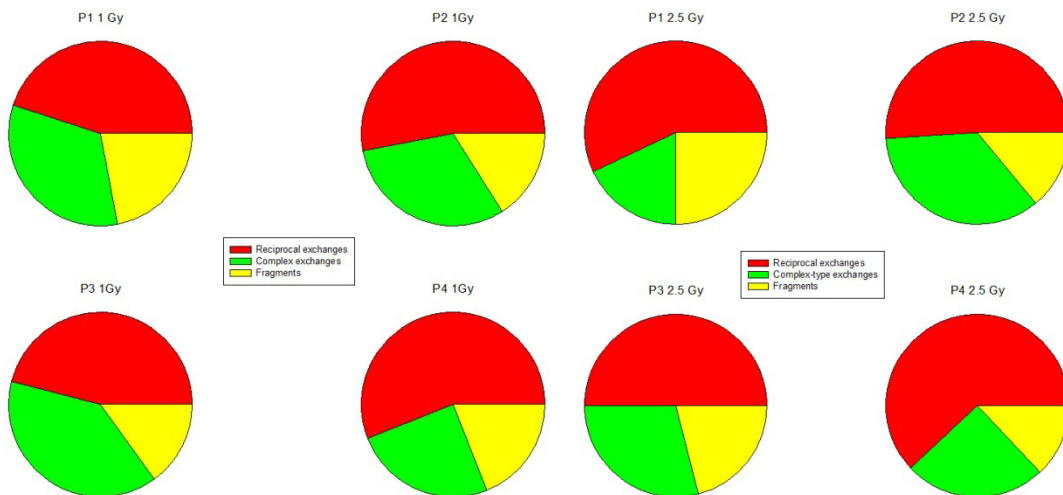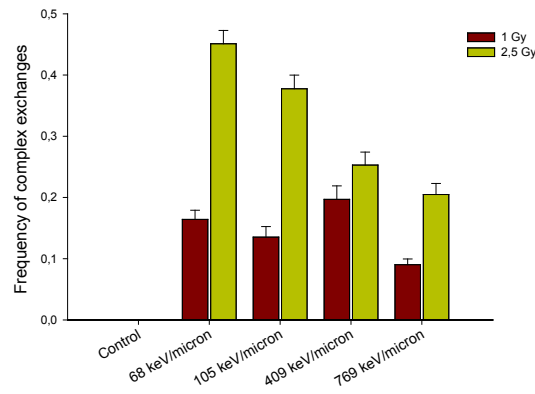
An example of mFISH scoring sheets is reported below (table 9). The analysis refers to samples irradiated with 1Gy of ^{16}O ions on position P1. Screenshots of the analysis process are shown in Fig. 32.

M 6 DSB	M 7 DSB	M 8 DSB	# of break/ cromosome	Involved chrosomomes	Aberration type

3			1	1. 1, 8, 8, 12, 15, X
				
				2. 1, 3, 8, 9, 15, 15
				
				3. 2, 2, 7, 5, 9, 11
					1. t(1;12)
					    t(8;15)*
					    t(8;X)
					2. t(1;15)
					    t(3;15)
					    t(8;9)*
					3. del 2 + ace 2
					    del 5 + ace 5
					    del 9 + ace 9
					    del 11 + ace 11
					    dic(2;7) + ace(2;7)

	1		1	4. 1, 4, 6, 7, 7, 12, 15	4. del 1 + ace 1
					    t(4;15)
					    dic(6;7) + ace (6;7)
					    dic(7;12)

	1		1 and 2 (complex exchange)	5. 5, 6, 7, 7, 8, 18, 19	5. del 6^c + ace 6^a
					    t(5;6^b;19)*
					    t(7;8)
					    t(7;18)

		2	1	6. 1, 1, 4, 7, 10, 11, 13, 14
				
				7. 1, 1, 4, 4, 6, 12, 18, X
					6. t(1;13)
					    t(1;10)
					    t(4;14)
					    t(7;11)
					7. t(6;X)
					    dic(1;4)
					    dic(1;18)
					    dic(4;12)

		2	1 and 2 (complex exchange)	8. 1, 2, 7, 9, 16
				
				9. 1, 6, 11, 11, 12, 17
					8. del 9
					    t(1^a;2^a)
					    t(1^b;2^b;16)*
					    t(1^c;7)*
					    t(2^c;6)
					9. del 1^b + ace 1^a
					    t(1^c;17)*
					    dic(6;12) + ace(6;12)
					    dic(11;11)

Table 9: Results of mFISH analysis for 9 PCC spreads following ^{16}O ions (INFN-LNS, Catania). M #° DSB indicates the number of breaks per PCC. Superscripts [a][b][c] indicates the resulting fragments, while t stands for reciprocal translocation, t* non-reciprocal trans location, del deletion, ace acentric fragment and dic dicentric.
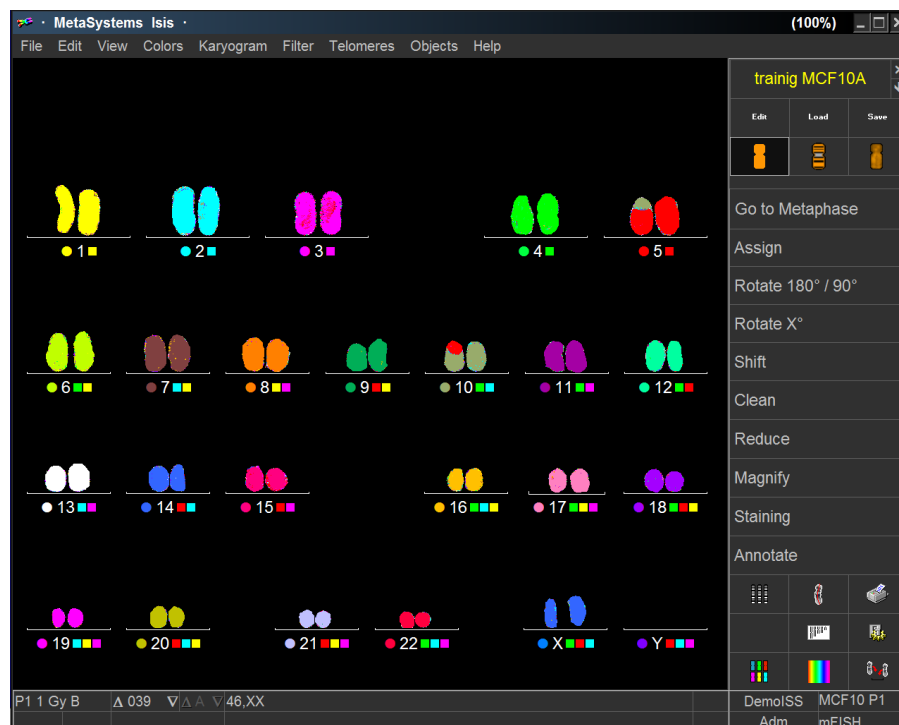
Fig. 32: The top figure illustrates a normal karyotype obtained after false colour processing of the categorized chromosomes. On the bottom, a translocation between chromosome 5 and 10 [t(5;10)] can be seen.

3. Preliminary conclusions and activities for 2013

- Our work demonstrated the feasibility for the Naples tandem to be used for curiosity-driven radiobiology research allowing investigation of end-of-track particles of intermediate Z
- There appears to be no significant difference in the cellular response in terms of clonogenic survival between reference x-ray radiation and protons or ^{12}C ion beams close to the Bragg peak, i.e. at very high LET values, which well agrees with established radiobiological models for this endpoint.
- However, qualitative and quantitative differences seem to exist as far as the induction of premature cellular senescence between x-rays and the charged particles thus far examined: At very high LET values, i.e. in the close proximity of the Bragg peak, this cellular response is more pronounced and persistent than seen after lower LET values
- Analysis of genetic damage in the form of structural chromosome aberrations confirms that complexity of damage is peculiar to ion irradiation and is much more effectively caused by this type of radiation compared to photons. As also seen for senescence, however, very high LET values, for which radiobiological effectiveness is predicted to decrease significantly, the levels of induced damage are consistently and significantly higher than after low-LET radiation.

An experimental run with ^{20}Ne ions will be carried out in February 2013 at INFN-LNS cyclotron. In June 2013 there will be also a PAC meeting at the latter facility where more the request for at least three more runs will be presented. Contacts have also been made with CNAO in Pavia to use the therapeutic ^{12}C beam.

4. Modellization work by Pavia Unit

During 2012 the Unit of Pavia, also using as a starting point previous works on modelling radiation-induced chromosome aberrations in human lymphocytes, developed a model and a MC code to simulate radiation-induced cell death, basing on an experimental study on AG1522 cells exposed to X rays [*Cornforth and Bedford 1987*], according to which some chromosome aberrations (Giemsa-stained dicentrics, rings and deletions, also called "lethal aberrations") lead to cell inactivation, and that chromosome aberrations derive from DNA cluster damage at the nm level ("Cluster Lesions", or CLs); the CL yield (average number of CLs per Gy per cell) was left as a semi-free parameter to be fixed after comparisons with experimental data. It was assumed that two CLs can produce aberrations only if they were induced within a threshold distance *d,* which is the second and last (semi-free) model parameter. Waiting for applying the model to the scenarios investigated by the unit of Naples, in the first part of 2012 a pilot study was performed on V79 cells exposed to photons, protons and ions of different energy; these cells were chosen because they provide a good response to variations in radiation quality, and have been used to characterize therapeutic beams including the proton beam of PSI (Switzerland), the Carbon beams of Chiba and GSI, and the proton and Carbon beams of CNAO. Figures 33 and 34 show, respectively, the model validation for cell inactivation by protons and carbon, as well as X rays: the simulated survival curves were compared with data relative to five proton beams (of energy 5.01, 3.20, 1.41, 0.76 and 0.64 MeV, corresponding to LET values of 7.7, 11.0, 20.0, 30.5 e 34.6 keV/μm) [*Belli et al. 1998*] and to four carbon beams (of energy 4.2, 11.0, 76.9 e 266.4 MeV/u, corresponding to LET values of 339.1, 153.5, 32.4 and 13.7 keV/μm) [*Weyrather et al. 1999*].

Concerning the parameter values, for protons a good agreement with the data was obtained with d=5 micron (for all energies) and with CL yields in the range 2 ÷4 CLs per Gy per cell (increasing with LET), whereas for carbon we used d=4 micron (for all energies) and CL yields in the range ~2 ÷6 CLs per Gy per cell (increasing with LET); a slightly smaller d for the carbon set was expected, since the cells used for the carbon experiments are slightly smaller *(W. Weyrather, personal communication)*: the ratio between the two d values (5/4=1.25) reflects the ratio between the two nuclear radii (6/5=1.20). Fig 35, which shows the CL yields as a function of particle type and LET, reports the CL yields used to obtain the proton and carbon survival curves reported in figs. 33 and 34. The very good agreement between simulations and data allowed validating the model and supported the assumptions on the underlying biophysical mechanisms; in particular, at least up to few Gy, dicentrics, rings and deletions were lethal not only for AG1522 cells exposed to X rays, as already reported in the literature, but also for V79 cells exposed to protons and carbon ions. Furthermore, the derived CL yields indicate that the critical DNA lesions for cell death are more complex than "clean" DSBs, which are in the order of 40 DSBs per Gy per cell. After validation, the model was used to characterize the dependence of cell inactivation on radiation quality. The results are shown in fig. 36, which reports the fraction of inactivated cells predicted for V79 cells exposed to 2 Gy protons or carbon having many different LET values, including values not considered in the experimental papers. As an hadrontherapy application, the model was applied to predict cell death by a carbon beam used for preclinical experiments at HIMAC in Chiba in the biology cave, where the beam delivery system is similar to the horizontal therapeutic line. To "calibrate" the two parameters, the simulated survival curves were compared with survival data obtained at HIMAC exposing V79 cells to two monoenergetic carbon beams (290 MeV/n and 135 MeV/n, corresponding to LET values of 13 keV/μm and 24 keV/μm), as well as gamma rays [*Belli et al. 2008*]. The comparison with the gamma curve confirmed d=5 micron; a good agreement with the two monoenergetic beams was obtained with 2.0 and 2.2 CLs per Gy per cell, respectively. Afterwards, the simulated survival curves were compared with data obtained at HIMAC for V79 cells at three depths along a 290 MeV/n carbon SOBP: 84, 111 and 131 mm, corresponding to dose-averaged LET of 40, 50 and 75 keV/μm, respectively. CL yields of 3.4, 3.6 and 4.7, respectively, led to a good agreement with the data. The HIMAC results are shown in fig. 37.

After this calbration step, the model was applied to the simulation of cell death in different positions along the aforementioned carbon SOBP, including positions not investigated in the experimental work. The results are reported in fig. 38, which shows the predicted inactivation fraction as a function of depth in water, as well as the corresponding (normalized) doses. The predicted cell death was basically constant along the SOBP, suggesting that the model may be applied to predict cell death by therapeutic beams also in SOBP positions for which experimental data are not available. More generally, these results suggest that Giemsa dicentrics, rings and deletions can be regarded as a "biological dose" that may be used as an effectiveness indicator for different beams, including therapeutic ones.

This pilot study allowed clarifying some important mechanisms governing the action of charged particles in DNA/chromosomes and cell inactivation, and allowed simulating cell death induced by protons and carbon ions of different energies. Furthermore, we developed a predictive tool that in some minutes can simulate the inactivation of V79 cells exposed to a given dose of protons or carbon ions with a given energy. The model avoids the use of RBE, which has the drawback of being subject to many variations depending on different factors, and is therefore a source of uncertainty. The

results described above were reported in a paper submitted to *Radiation Research* at the end of 2012, which was accepted at the beginning of 2013 (Ballarini et al., *in press*). In view of the application to the results obtained by the unit of Naples, in the second part of 2012 the unit of Pavia extended the approach to human cells, in particular AG1522 fibroblasts. As a first step the target nuclei were modelled as circular cylinders; in 2013 this representation will be refined implementing a cylinder with elliptical base, which is more realistic. The first results of cell death, shown in fig. 39, showed a very good agreement with the original data of Cornforth and Bedford, who characterized the link between lethal aberrations and cell inactivation for AG1522 fibroblasts exposed to X rays; in 2013 the approach will be applied to data obtained by the Naples unit exposing this cell line (and possibly also other lines) to different ions, as well as photons for comparison.
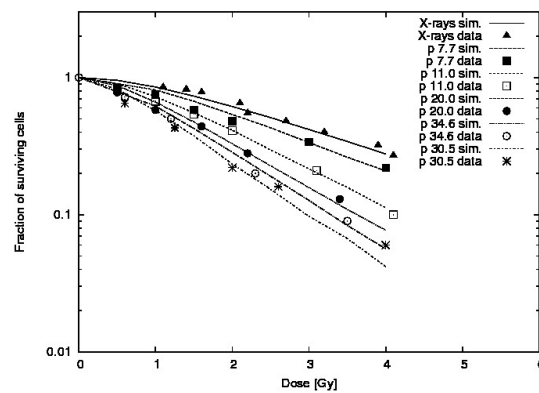

Fig 33: Survival of V79 cells exposed to five proton beams of different energy, as well as X rays for comparison; the lines are simulation results, the points are experimental data.
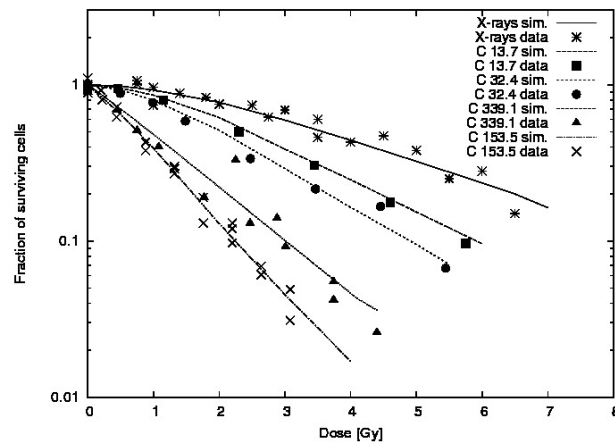

Fig. 34: Survival of V79 cells exposed to four carbon beams of different energy, as well as X rays for comparison; the lines are simulation results, the points are experimental data.
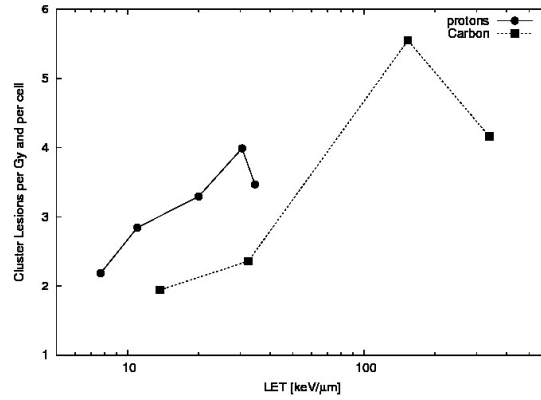
Fig.35. Average number of CLs per Gy per cell used as model input to obtain the proton and carbon curves reported in figs. 33 and 34. The points are the CL yields for protons (circles) and carbon (squares), the lines are guides for the eye.
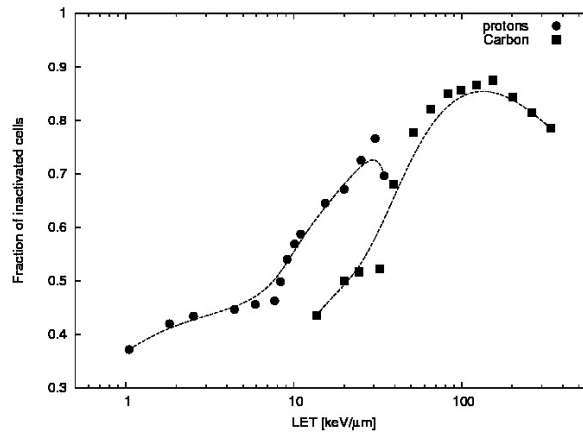

Fig. 36: Inactivation fraction simulated for V79 cells exposed to 2-Gy protons (circles) and carbon (squares); the lines are guides for the eye.
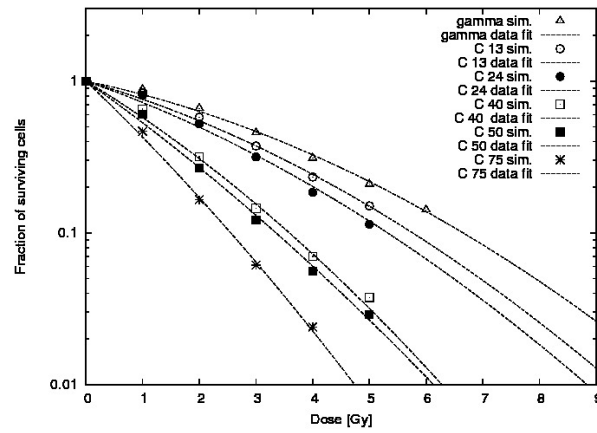
Fig.37: V79 survival for gamma rays (for comparison), two monoenergetic carbon beams (LET: 13 and 24 keV/μm), and three positions along a carbon SOBP (corresponding LET: 40, 50 and 75 keV/μm). The points are simulation results, the lines are data fits relative to pre-clinical experiments performed at HIMAC in Chiba.
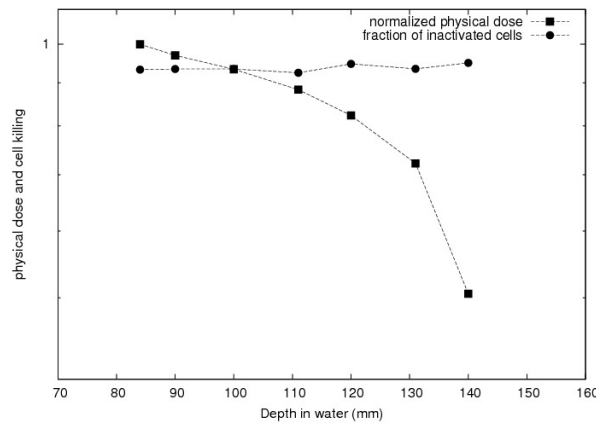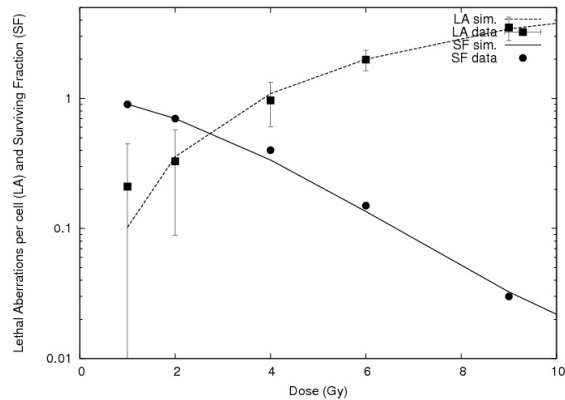

Fig. 39: Predicted inactivation for V79 cells exposed to different depths along a carbon SOBP at HIMAC (circles); the squares are the corresponding (normalized) physical doses. In both cases the lines are guides for the eye.

FIG 39: Surviving fraction and average number of lethal aberrations per cell for AG1522 human fibroblasts exposed to X rays. The lines are simulation results, the points are experimental data.

The references for this paragraph are listed below.

1. Cornforth M, Bedford J. A quantitative comparison of potentially lethal damage repair and the rejoining of interphase chromosome breaks in low passage normal human fibroblasts. Radiat Res 1987; 111:385-405.
2. Belli M, Cera F, Cherubini R, Dalla Vecchia M, Haque AMI, Ianzini F, et al. RBE-LET relationship for cell inactivation and mutation induced by low energy protons in V79 cells: further results at the LNL facility. Int J Radiat Biol 1998; 74:501-509.
3. Weyrather WK, Ritter S, Scholz M, Kraft G. RBE for Carbon track-segment irradiation in cell lines of differing repair capacity. Int J Radiat Biol 1999; 75:1357-1364.
4. Belli M, Bettega D, Calzolari P, Cherubini R, Cuttone G, Durante M, et al. Effectiveness of monoenergetic and Spread-Out Bragg Peak Carbon ions for inactivation of various normal and tumour cell lines. J Radiat Res 2008; 49:597-607.
5. Ballarini F, Altieri S, Bortolussi S, Giroletti E, Protti N. A model of radiation-induced cell killing: insights into mechanisms and applications for hadrontherapy. Radiat Res, in press.